ELSEVIER

Budgets of turbulent stresses and fluxes in a vertical slot natural convection flow at Rayleigh Ra = 10^5 and 5.4 10^5

R. Boudjemadi,* V. Maupu,* D. Laurence,* and P. Le. Quéré†

*EDF Laboratoire National d'Hydraulique, Chatou, France and
†LIMSI, CNRS, Orsay, France

A direct numerical simulation (DNS) of natural turbulent convection in a differentially heated infinite vertical slot has been computed with a mixed finite difference/Fourier code at Rayleigh numbers of $R_a = 1.0\ 10^5$ and $R_a = 5.4\ 10^5$. A database containing up to second-order budgets has been collected, and the physics of the Reynolds stresses and turbulent heat fluxes is analyzed in light of the relevant conservation equations. Unusual features are the negative production terms and countergradient turbulent transport. Near-wall flow characteristics are strongly influenced by transport of quantities from the core of the "Couette flow" where most of the turbulence is produced. A fairly simple second-moment closure, relying on elliptic relaxation instead of damping functions for near wall effects, is found to perform fairly well on a global scale. Although the modeling approach is open for improvements if a term-by-term analysis is conducted. © *1997 by Elsevier Science Inc.*

Keywords: natural convection; direct numerical simulation; second moment modelling

Introduction

The problem addressed here is the simple and ubiquitous natural convection flow inside double glazed windows, not for the sake of building insulation, but for providing a database against which turbulence models can be compared in a simple one-dimensional problem (1-D) (in the Reynolds-averaged sense). In the power generation industry, for example, many of the computational fluid dynamics (CFD) applications concern near-wall heat transfer predictions in the presence of gravity forces. Also, relying on heat removal through natural convection in future plants, instead of forced convection, can further enhance safety.

Much progress has been achieved in realistic modeling of unknown dynamic terms in second-moment closures (Craft et al. 1991, Launder et al. 1991, Durbin, 1993. So et al. 1991) thanks to databases obtained from direct numerical simulations (DNS) in isothermal flows. Little data are available concerning turbulent heat fluxes in wall-bounded flows, with the exceptions of Kasagi et al. (1992), Lyons et al. (1991), and Maupu et al. (1993).

Concerning the natural convection case, to extend the laminar and transitional simulations of Lee and Korpela (1983), no DNS database was available when the present work began. It is difficult to perform experiments that assist in modeling, because ideal homogeneity in two directions (susceptible to 1-D modeling) and symmetry are nearly impossible to achieve. This lack of data has resulted in a fairly wide range of model formulations and the determination of constant values related to natural convection in the literature (Peeters and Henkes 1992). Very recently, however, Betts and Bokhari (1996) provided detailed measurements in a high-aspect ratio ($H/h = 28.6$) tall rectangular enclosure, exhibiting nearly perfect symmetrical and homogeneous (at midheight) profiles for Rayleigh numbers Ra = 8.6 10^5 and 14.3 10^5. Phillips (1996) obtained mean and second-order correlation results by means of a refined DNS at Ra = 0.056 10^5 and 0.157 10^5. The present DNS at higher Ra numbers, together with the independent computation of Vertsteegh and Nieuwstadt (personal communication, thesis to appear in 1996), also provides all the terms appearing in the budgets of the heat fluxes and the Reynolds stresses. This database was set up in an ensemble of electronic files for the "5th ERCOFTAC/IAHR Workshop on refined Flow modeling" (Laurence et al. 1996) and is available on request from D. Laurence.

Although we have discussed the interest in the present unstratified simulation, we should stress its limitations. It is well known that most real-life tall enclosures exhibit some stratification effects, because heat tends to accumulate in the upper region. This results in stratification effects that tend to dampen turbulence and separate the flow in a double boundary layer with a stagnant flow in the central region. Attempts by the present team to reproduce by DNS this kind of flow failed, because higher Ra numbers (and, thus, higher DNS mesh densities) are probably required for turbulence to develop against stratification.

The present DNS corresponds to a very tall enclosure with no stratification, again, a rare real-life situation, but one that is easily amenable to 1-D second-moment simulation, for which it provides valuable information. It must be stressed, however, that features of the present flow are largely dominated by the quasi-homogeneous shear appearing in the central part of the channel. Thus, present conclusions may not hold in general natural convection cases.

Address reprint requests to Dr. V. Maupu, EDF Laboratoire National d'Hydraulique, 6, quai Watier BP49, 78401 Chatou cedex FRANCE; R. Boujemadi can also be contacted at that address.

Received 10 March 1996; accepted 15 October 1996

Int. J. Heat and Fluid Flow 18: 70–79, 1997
© 1997 by Elsevier Science Inc.
655 Avenue of the Americas, New York, NY 10010

0142-727X/97/$17.00
PII S0142-727X(96)00144-5

Equations, flow configurations and notations

The incompressible Navier–Stokes equations using the Boussinesq approximation are written in nondimensional form and as deviations from a prescribed analytical basic laminar solution $(U^b_{1,3}, T^b)$:

$$\begin{cases} u_{i,i} = 0 \\ u_{i,t} + (u_j + U^b_j)u_{i,j} = -\dfrac{1}{\rho_0}p_{,i} + \left(\dfrac{1}{\mathrm{Gr}}u_{i,j}\right)_{,j} + \dfrac{1}{\mathrm{Gr}}\theta\delta_{i1} - u_j U^b_{i,j} \\ \theta_{,t} + (u_j + U^b_j)\theta_{,j} = \left(\dfrac{1}{\mathrm{Ra}}\theta_{,j}\right)_{,j} - u_j T^b_{,j} \end{cases}$$

These nondimensional equations and solutions depend only on:

Rayleigh number

$$\mathrm{Ra} = \frac{g\beta\,\Delta T D^3}{\nu\kappa}$$

Grashof number

$$\mathrm{Gr} = \frac{g\beta\,\Delta T D^3}{\nu^2}$$

where g, β, ν are, respectively, the gravity, the dilatation parameter, and kinematic viscosity. $D = 1$ is the gap width, $\Delta T = 1$ the temperature difference between walls, and the equations are solved for $\mathrm{Ra} = 10^5$ and $5.4\ 10^5$, while the Prandtl number is $P_r = \nu/\kappa = 0.71$. A reference buoyancy velocity can be defined as $V_b = g\beta\,\Delta T D^2/\nu$, $(V_b = R_a\kappa/D)$.

The ratio of the friction velocity u^* (which will be used for normalizing the results) and the reference buoyancy velocity V_b is:

$$u^*/V_b = 4.94\ 10^{-4} \quad \text{and} \quad u^*/V_b = 1.637\ 10^{-4}$$

for the lower and higher Rayleigh number, respectively. Similarly, temperatures will be normalized by $\theta^* = \kappa/u^* \cdot dT/dz|_{\mathrm{wall}} = 0.0515\,\Delta T$ and $0.0582\,\Delta T$, respectively. Budgets of the Re stresses, turbulent heat fluxes and temperature variance are normalized respectively by u^{*4}/ν, $u^{*3}\theta^*/\nu$, $u^{*2}\theta^{*2}/\kappa$. Subscripts are used for the velocity components with directions 1, 2, 3 corresponding to x, y, z, respectively, where x is the (vertical) streamwise coordinate, y is the spanwise coordinate and z is the wall normal coordinate.

Numerical method

The equations given in the previous section are solved using a mixed spectral/finite difference approach (see Grötzbach and Wörner 1992) and Schumann's (1984) combined fast Fourier transform (FFT) tridiagonal system solver. For time integration, a fractional step scheme is used: Convection; Diffusion + Gravity terms + Sources terms; Pressure increment + Continuity.

An Adams–Bashforth scheme is used for the convection step and a Crank–Nicolson scheme for the diffusion step. The nonlinear or convection term is computed in the physical space under the semiconservative form and discretized in fourth-order finite differences. For the two other steps, space derivatives in the homogeneous direction x and y are obtained by FFTs. Derivatives in the wall-to-wall direction are then discretized with a standard second-order finite-difference scheme. Pressure and velocity nodes are staggered (no pressure boundary condition is required for the latter).

A large number of points is used in the wall-to-wall direction to balance the difference in accuracy between Fourier and finite-difference discretizations. A standard hyperbolic tangent distribution of nodes yields a strong clustering of nodes near the wall. Several tests using different resolutions and domain sizes, and converging statistics up to second moments, yielded very similar results to the case presently described, and using $(n_x = 128,\ n_y = 32,\ n_z = 128)$ points for a computational domain of $(L_x = 2.5,\ L_y = 1.,\ L_z = 1.)$.

Results

The flow characteristics are different from those of a standard channel or boundary-layer flow. For the dynamics, 90% of the channel width is occupied by a quasi-constant turbulent shear or "Couette" flow, while the remaining near-wall flow is highly viscous. As will be seen from the budgets, this Couette flow is the turbulence generator, because shear and gravity production terms remains very large at the centre.

First and second moments are shown in Figure 1 with the lower $\mathrm{R_a}$ values plotted on the left and the higher $\mathrm{R_a}$ values plotted on the right half of the figure. Apart from the increase of the near-wall slope, the change on the mean quantities with $\mathrm{R_a}$ is fairly small, with the present scaling on wall fluxes of momentum u^* and heat θ^*. The corresponding Nusselt number values for the channel walls are 2.62 and 5.15, showing that molecular heat transfer is still significant. However, at the higher-$\mathrm{R_a}$, the rms of the vorticity components are equal in the central part of the channel, showing isotropy of the small scales. The Reynolds stresses and fluxes also tend to become more isotropic at the higher $\mathrm{R_a}$, even though the streamwise velocity fluctuations remain significantly larger than the other normal components at the center of the channel; and higher than one would expect from a "Couette" flow, a feature attributed here to the gravity production term. A ratio of streamwise to wall-normal fluctuations of about 1.8 was also found by the DNS of Phillips (1996) and the experiment of Betts and Bokhari (1996).

Note that there is no change of sign (in opposition to the velocity gradient) in the shear stress, in agreement with the data of Phillips (1996). The present observation should not be extrapolated to remove an experimental uncertainty concerning a possible shear stress change of sign in the natural convection vertical boundary layer (Tsuji et al. 1991; Kato et al. 1993; Karlsson et al. 1990). For a single heated plate, the outer flow is able to develop with a milder velocity profile; whereas, in the present confined flow, transport effect prevents the change of sign in the shear stress near the wall, as will be seen form the budgets.

Although in a shear flow from the normal stress component is smaller than the spanwise, the equality of both normal stresses at the center is somewhat surprising. However, this finding is also present in the data of Versteegh and Nieuwstadt and, to a lesser degree, in the data of Phillips (1996) which, nonetheless, also show a slight hump at the center for the spanwise component).

Finally, considering the heat fluxes, we notice a large streamwise component generated by the combination of the wall-to-wall flux and the mean velocity gradient, and as will be seen from the budgets, it allows gravity to make a significant contribution. To illustrate these effects, we recall that the Reynolds-stress balance equations are traditionally written as:

$$\frac{\partial \overline{u_i u_j}}{\partial t} + U_k \frac{\partial \overline{u_i u_j}}{\partial x_k} = P_{ij} + G_{ij} + \Phi_{ij} + T_{ij} + D_{ij} - \varepsilon_{ij} \qquad (1)$$

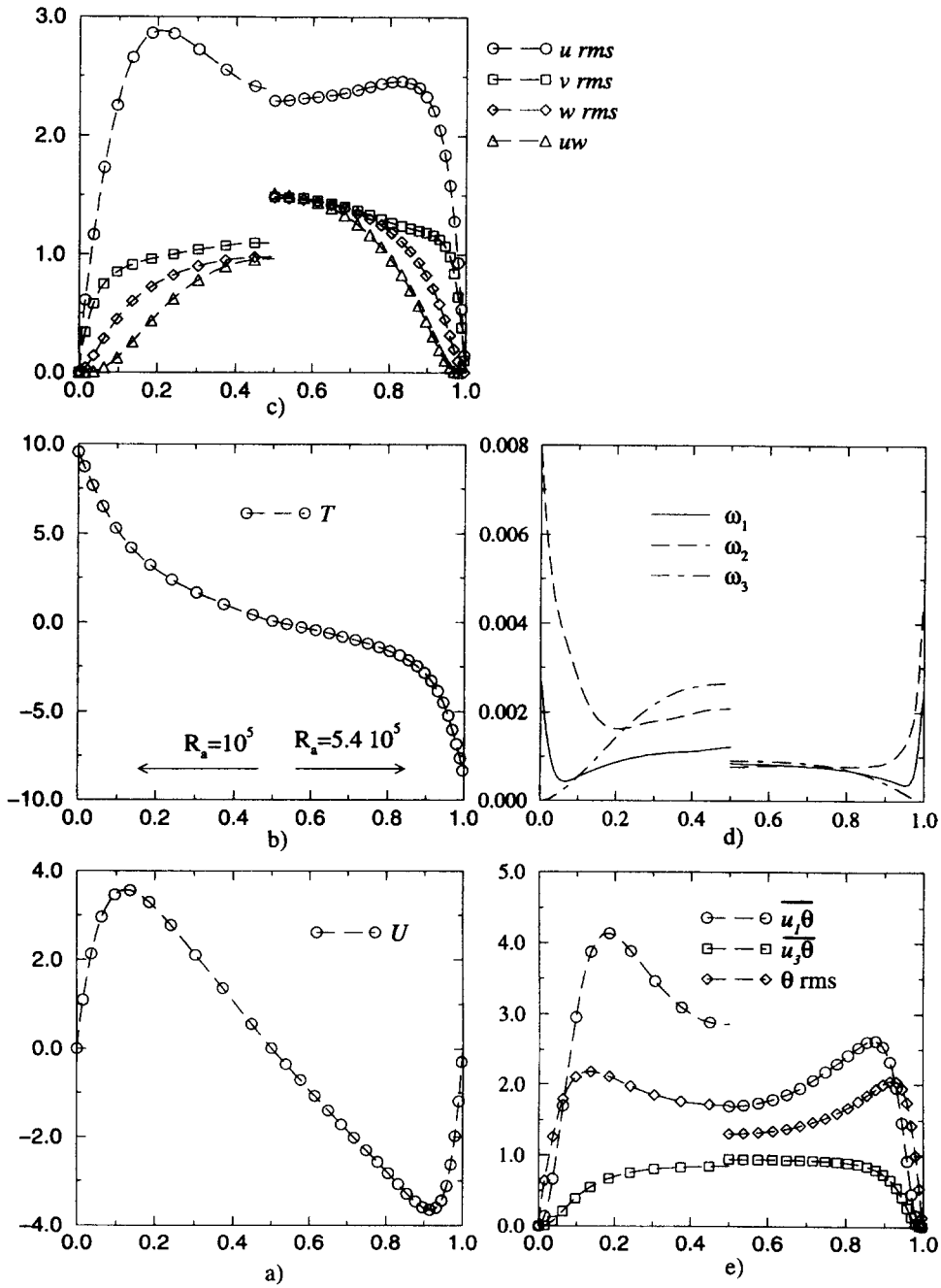

Figure 1 First and second moments: a) mean velocity; b) mean temperature; c) velocity fluctuations; d) vorticity fluctuations; e) heat fluxes and temperature fluctuations

with gradient production, gravity production, velocity pressure-gradient correlations, turbulent diffusion, viscous diffusion, and dissipation, respectively, on the right-hand side. Similarly, the turbulent heat flux balance equations are written as:

$$\frac{\overline{\partial u_i\theta}}{\partial t} + U_k\frac{\overline{\partial u_i\theta}}{\partial x_k} = \underbrace{-\overline{u_iu_k}\frac{\partial\Theta}{\partial x_k} - \overline{u_k\theta}\frac{\partial U_i}{\partial x_k}}_{P_{i\theta}} + \underbrace{\beta g(\overline{\theta^2}\delta_{i1})}_{G_{i\theta}} \underbrace{-\frac{1}{\rho}\theta\frac{\overline{\partial p}}{\partial x_i}}_{\Phi_{i\theta}}$$

$$\underbrace{-\frac{\partial}{\partial x_k}\overline{u_i\theta u_k}}_{T_{i\theta}} + \underbrace{\frac{\partial}{\partial x_k}\left[\kappa u_i\frac{\overline{\partial\theta}}{\partial x_k} + \nu\theta\frac{\overline{\partial u_i}}{\partial x_k}\right]}_{D_{i\theta}}$$

$$\underbrace{-(\nu+\kappa)\frac{\overline{\partial u_i}}{\partial x_k}\frac{\partial\theta}{\partial x_k}}_{\varepsilon_{i\theta}} \qquad (2)$$

Note that, as for the "velocity pressure-gradient correlations", $\Phi_{i\theta}$ is not the usual "pressure scrambling" term ("pressure-temperature-gradient correlation") since the "temperature-pressure-gradient correlation" was not decomposed into "pressure diffusion" and "pressure-temperature-gradient correlation" contributions. Indeed, it will be seen that this decomposition only confuses the budget profiles, and "pressure–strain" or "pressure-scrambling" models actually compare better to the original pressure–gradient-related correlations.

For the present flow, statistically stationary and homogeneous in the mean flow direction, the left-hand sides of Equations 1 and 2 are identically zero, while all production terms are detailed below (with $\beta g > 0$):

$$P_{11} + G_{11} = -2\overline{u_1u_3}\frac{\partial U_1}{\partial x_3} + 2\beta g\overline{u_1\theta}$$

$$P_{13} + G_{13} = -\overline{u_3u_3}\frac{\partial U_1}{\partial x_3} + \beta g\overline{u_1\theta}$$

$$P^T_{3\theta} = -\overline{u_3u_3}\frac{\partial T}{\partial x_3}$$

$$P^U_{1\theta} + P^T_{1\theta} + G_{1\theta} = -\overline{u_3\theta}\frac{\partial U_1}{\partial x_3} - \overline{u_1u_3}\frac{\partial T}{\partial x_3} + g\beta\overline{\theta^2}$$

$$P_{\theta\theta} = -2\overline{u_3\theta}\frac{\partial T}{\partial x_3} \qquad (3)$$

Stress budgets

Budgets of the Reynolds stresses are displayed in Figures 2 and 3, again with the lower R_a on the left and the higher R_a on the right half of the figure. We notice that for the latter, the turbulence is sufficiently developed for the viscous diffusion term to be negligible in the central part of the channel.

The budget of the shear stress, $\overline{u_1u_3}$, shows that most of the shear production takes place in the central part of the channel. Near the wall, this term becomes negative as the velocity gradient changes sign (but not the shear stress). The shear stress remains positive because of the gravity production, which is proportional to the large vertical heat flux. Turbulent transport reinforces this feature. The off-diagonal component of dissipation is far from negligible, even in the central part of the channel, in opposition to what is assumed for high-Re flows.

The budget of the streamwise velocity fluctuation $\overline{u_1u_1}$ is similar to that of the shear stress. The Couette flow is dominated by shear production, while gravity production dominates as the velocity gradient changes sign near the wall. This near-wall layer again experiences negative turbulent kinetic "production" ($P = 1/2P_{11}$) because of the constant sign of the shear stress. Turbulence is equally sustained by gravity production and turbulent transport, the latter opposite to the molecular diffusion term, meaning the countergradient turbulent transport is taking place (i.e., transport makes a positive contribution in the wall layer, where the longitudinal Reynolds stress is already maximum).

Positive gravity production is a consequence of the relatively strong streamwise heat flux (which would be predicted as zero in a simple eddy-diffusivity model) and seems to compensate for low or negative shear production, also missed by eddy-viscosity models. This compensation explains why low-Re k–ε models behave better in natural convection flows than in other flows similarly affected by body forces (stratification or rotation).

The wall-normal and spanwise diagonal components of the Reynolds-stress tensor are generated by the velocity–pressure-gradient correlations, draining energy form the streamwise diagonal component. As noted earlier, the fact that at the channel center the normal and spanwise velocity fluctuations are of similar magnitude is surprising and is a consequence of the similar levels of the velocity–pressure-gradient correlations (the pressure-transfer component associated with gravity will equally redistribute energy among normal and spanwise fluctuations, but not that associated with shear production, which is expected to be dominant). Near the wall, where the wall-normal fluctuations are impeded, reverse transfer of energy from the wall-normal to the other two components occurs. Transport of the wall-normal energy must be higher to compensate for this effect, but then dissipation for the wall-normal component is smaller at the center, resulting as noticed, in similar magnitudes for the normal and spanwise Reynolds stresses.

The pressure-transport terms are non-zero only for $\overline{u_1u_3}$ and $\overline{u_3u_3}$. The split of "velocity–pressure-gradient correlations" into "pressure strain" and "pressure diffusion" is shown separately in Figure 4. Pressure diffusion is, on the average, opposite to turbulent diffusion and pressure strain. The "velocity–pressure-gradient correlations" can be seen to be easier to model than the "pressure strain". This, in effect, is what is represented by the models, because pressure diffusion is usually not modeled.

Heat-flux budgets

In the $\overline{u_3\theta}$ budget (Figure 4), production is roughly balanced by the pressure-scrambling term. For the high-Ra case, the viscous diffusion term and turbulent transport term behave as gradient transport terms, helping $\overline{u_3\theta}$ to remain positive, in the vicinity of the wall for the turbulent term and even closer to the wall for the viscous term.

The budget of the vertical heat flux $\overline{u_1\theta}$ is similar to that of $\overline{u_1u_3}$. It seems that for both, dissipation is never negligible, this quantity approximately balancing the gravity production. Surprisingly, this feature is unchanged when the Rayleigh number increases; whereas, the dissipation of $\overline{u_3\theta}$ clearly decreases. We might explain nonvanishing viscous effects on $\overline{u_1\theta}$ by the fact that gravity maintains a non-zero correlation between temperature and vertical motion at all scales.

The near-wall value of the $\overline{u_1\theta}$ dissipation term is seen to be near zero, which is significantly different from the nonbuoyant channel flow DNS results of Kasagi et al. (1992). Although there is no theoretical reason for this value to be zero, this can be attributed to the fact that the $\overline{u_1\theta}$ heat flux itself goes to zero at the wall as rapidly as $\overline{u_3\theta}$ in connection with the negative gradient production term. In contrast with the nonbuoyant chan-

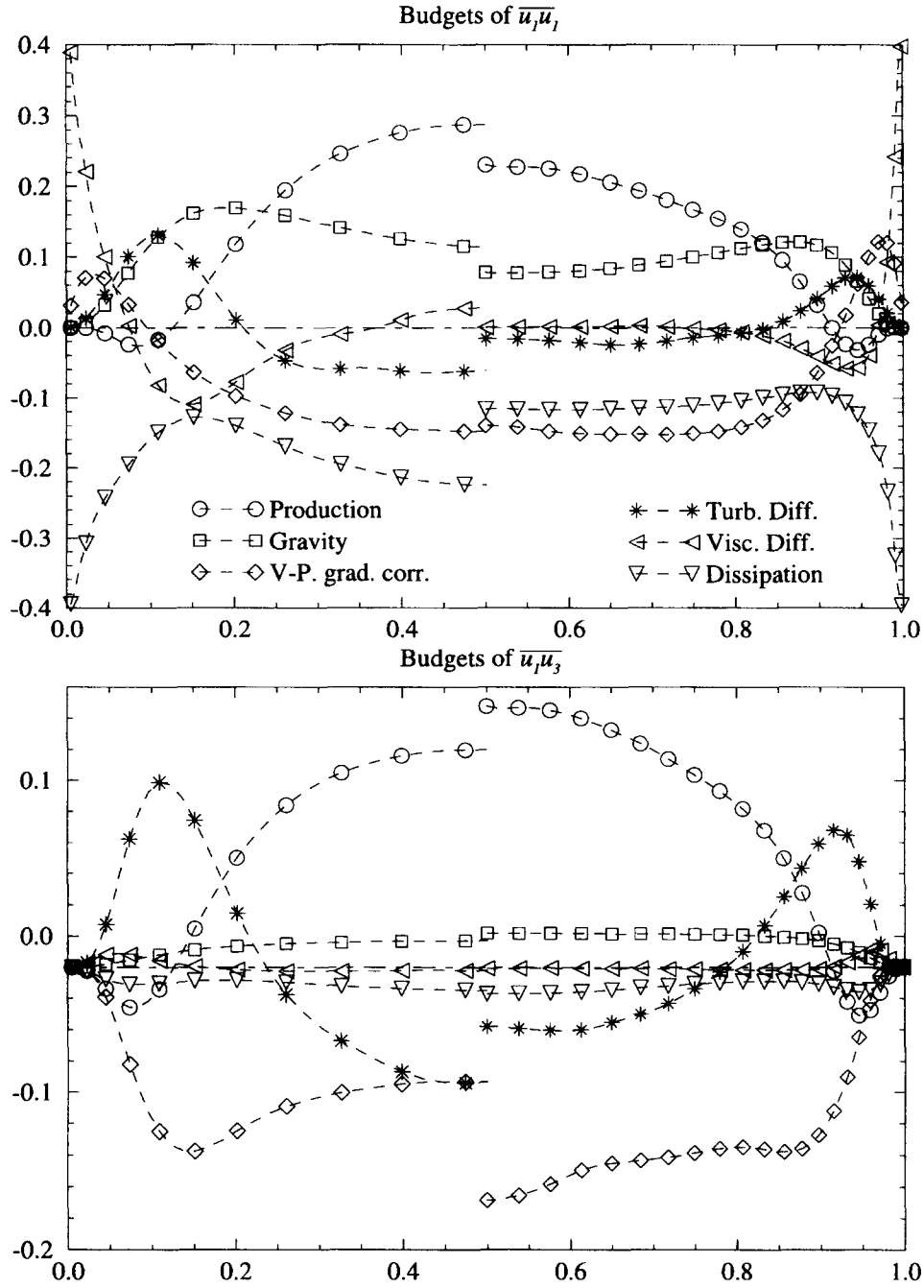

Figure 2 Budgets of the streamwise and shear components of the Reynolds stresses

nel flow case, the heat flux is produced here mainly in the central Couette flow.

In the central region, the production term seems to be very sensitive to the Rayleigh number, and this is also reflected by a factor of 2 in $\overline{u_1\theta}$, as seen in Figure 1e. Note that by conservation of the wall-to-wall total heat flux, $\overline{u_3\theta}$ scaled by $u^*\theta^*$ will tend to unity. Hence, the production of $\overline{u_1\theta}$ decreases like the temperature gradient. On the other hand, because the shear stress increases and the velocity gradient decreases while increasing the Rayleigh number, the production of $\overline{u_3\theta}$ remains fairly unchanged.

Returning to Figure 1, the lower Ra case shows a significant maximum of the vertical velocity fluctuation and heat flux near the wall ($z/D = 0.2$). On the other hand, the turbulent diffusion term behaves somewhat in opposition to standard gradient-diffusion models; i.e., $\overline{u_1\theta}$ and $\overline{u_1u_3}$ are transported from the central region, where they show a minimum, to the near-wall region where they show a maximum. The reality of this curious behaviour is backed up by the fact that such results could be better reproduced by a model including the production terms in the triple correlation budgets, as shown in Boudjemadi (1996) and Boudjemadi et al. (1996).

Assessment of the database

The major features of the present results have been confirmed by an independent DNS by T. Versteegh and F. Nieuwstadt (personal communication, thesis to appear in 1996); namely, the non-negative value of the near-wall shear stress, distributions of

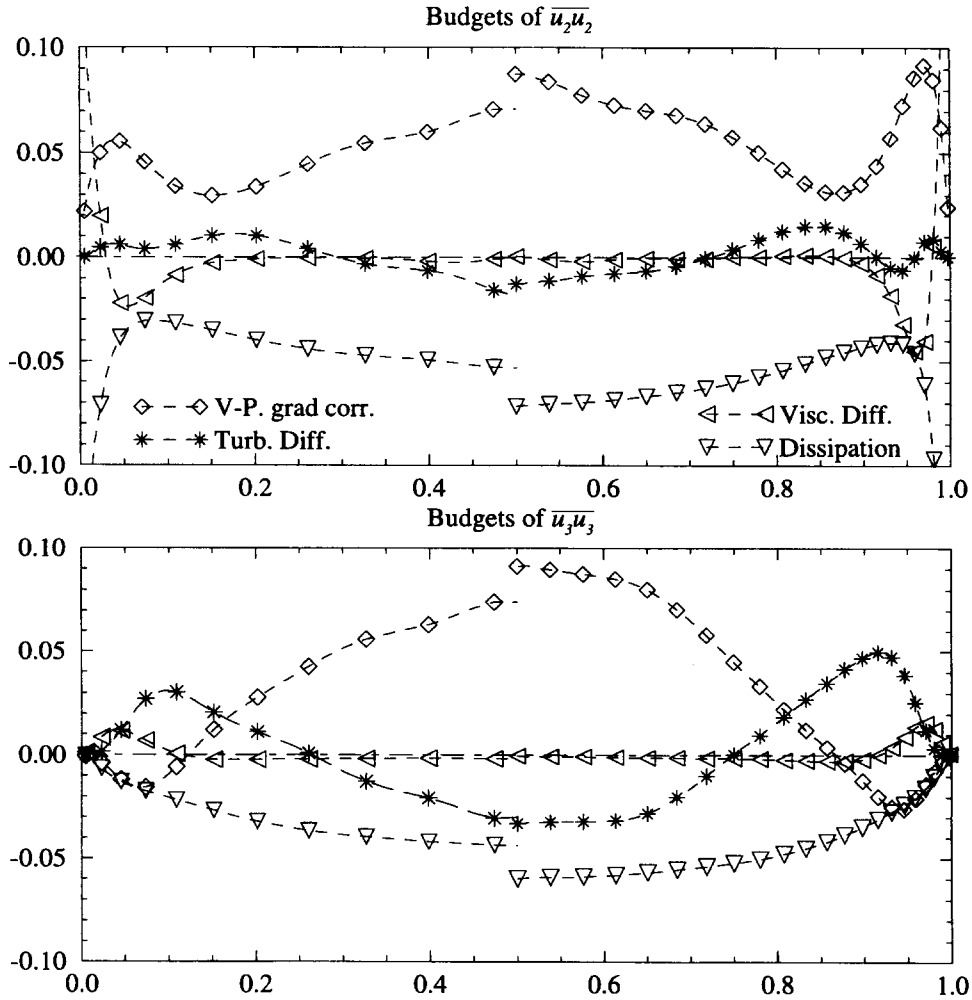

Figure 3 Budgets of the spanwise (top) and wall-normal (middle) Reynolds stresses

all production terms, and the nonvanishing heat-flux dissipation (especially for the vertical flux). Differences lie in the wall values of the viscous terms in the heat-flux budgets and in the turbulence intensities, which were found slightly higher in the wider computational domains used by the Dutch team. The latter could be due to the fact that imposing a zero global mass flux in a domain that is too narrow in the spanwise direction may prevent low-frequency fluctuations. On the other hand, the former difference could be attributed to the finer grid of the present computation (Figure 5).

The fairly good agreement of the present data, except for the temperature variance, with the recent experiment of Betts and Bokhari (1996) at a slightly higher Ra value of 8.5 10^5 is shown in Figure 6.

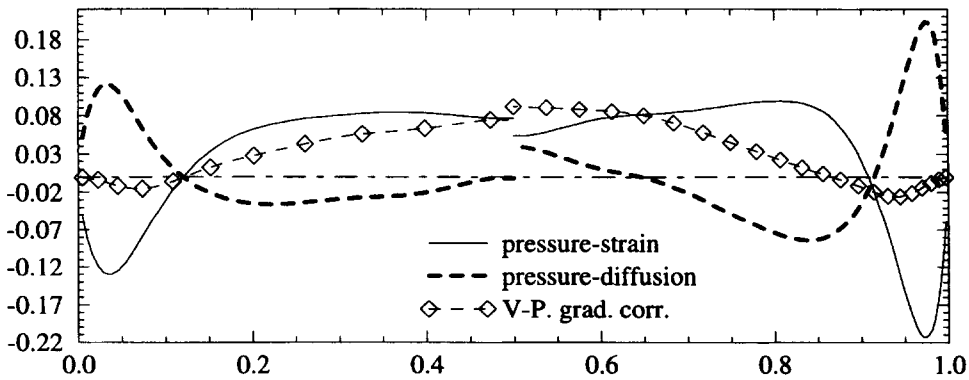

Figure 4 Split of the velocity pressure-gradient correlation for u_3u_3

Modeling considerations

As mentioned in the Introduction, no consensus has yet been reached for a "standard" second-moment closure for natural convection flows. For a first comparison the elliptic relaxation (nonbuoyant) model of Durbin (1993) was chosen. The approach avoids using damping functions and recovers the blocking effect that the wall imposes to the normal fluctuations, by processing any homogeneous pressure–strain model through the following elliptic operator.

$$L^2\nabla^2\frac{\varphi_{ij}}{k} = \frac{\varphi_{ij} - \varphi_{ij}^h}{k} \qquad \text{with}$$

$$L = C_L \max\left[\frac{k^{3/2}}{\varepsilon}, C_n\left(\frac{\nu^3}{\varepsilon}\right)^{1/4}\right] \tag{4}$$

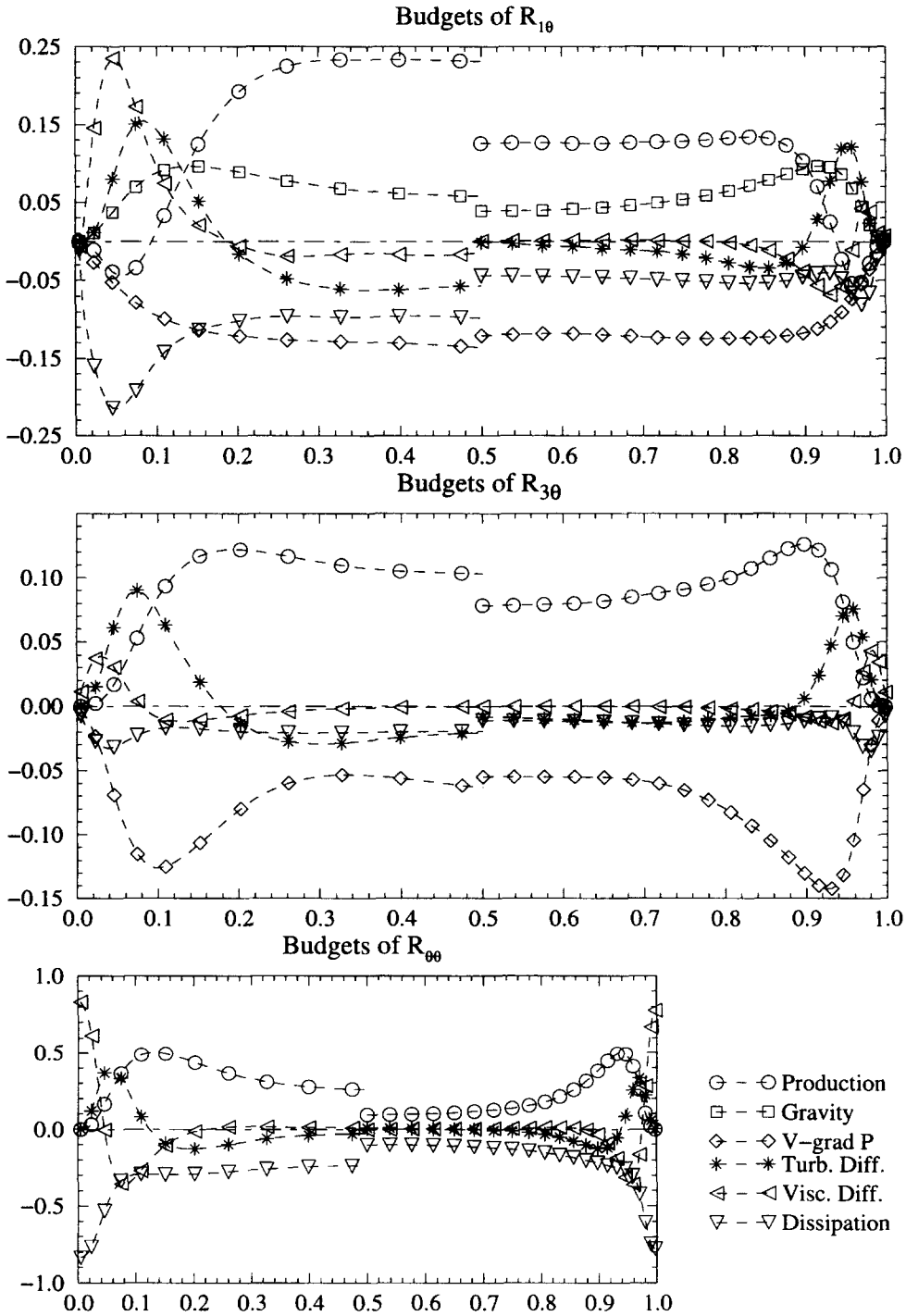

Figure 5 Budgets of the turbulent heat fluxes and temperature variance

Here, the "IP" model was used:

$$\varphi_{ij}^{h} = -c_1 \mathrm{dev}(\overline{u_i u_j})\frac{\varepsilon}{k} - c_2 \mathrm{dev}(P_{ij}) \tag{5}$$

Note that in the present approach, φ_{ij} is considered to represent not only the classical pressure strain Φ_{ij}, but also pressure transport and the difference between stress anisotropy and dissipation anisotropy. Indeed, dissipation is modelled as

$$\varepsilon_{ij}|_{\mathrm{mod}} = \frac{\varepsilon}{k}\overline{u_i u_j} \qquad \text{instead of} \qquad \varepsilon_{ij}|_{\mathrm{mod}} = \varepsilon\frac{2}{3}\delta_{ij}$$

$$\varphi_{ij} \xrightarrow[\text{(represents)}]{} \Phi_{ij} + \frac{2}{3\rho}\frac{\partial \overline{p u_k}}{\partial x_k}\delta_{ij} + \left(\frac{\varepsilon}{k}\overline{u_i u_j} - \varepsilon_{ij}\right) \tag{6}$$

According to Durbin (1993), (see also Rodi and Mansour 1990), the primary effect of a wall is the reduction of the wall-normal velocity fluctuation; thus, once this feature is captured, further damping of the pressure-scrambling terms of the heat-flux equation is not a necessity. For simplicity, the standard linear model was used (without relaxation):

$$\varphi_{i\theta} = -\left(C_{\theta_1}\frac{\varepsilon}{k}\right)\overline{u_i\theta} + C_{\theta_2}\overline{u_k\theta}\frac{\partial U_i}{\partial x_k} - C_{\theta_3}\beta g_i\overline{\theta^2} \tag{7}$$

The classical gradient diffusion hypothesis is used for all transport terms, e.g.

$$\frac{\partial(\overline{u_i\theta_{u_3}})}{\partial x_3} = \frac{\partial}{\partial x_3}\left(\frac{C_\mu \overline{u_3 u_3} T}{\sigma_\theta}\right)\frac{\partial \overline{u_i\theta}}{\partial x_3} \tag{8}$$

As for the length scale, a Kolmogorov bound appears in the time scale, but is only active in the very near-wall region

$$T = \max\left[\frac{k}{\varepsilon}, C_T\left(\frac{\nu}{\varepsilon}\right)^{1/2}\right] \tag{9}$$

An equation for $\overline{\theta^2}$ is needed, and is written as

$$\frac{\partial\overline{\theta^2}}{\partial t} = -2\overline{u_3\theta}\frac{\partial T}{\partial x_3} + \frac{\partial}{\partial x_3}\left(\kappa + \frac{C_\mu\overline{u_3u_3}T}{\sigma_\theta}\right)\frac{\partial\overline{\theta^2}}{\partial x_3} - \varepsilon_\theta \tag{10}$$

with an algebraic expression for the variance dissipation

$$\varepsilon_\theta = \frac{1}{R}\frac{\overline{\theta^2}}{T} \tag{11}$$

following Haroutunian and Launder (1988)

$$R = \frac{1}{1.5(1+A_{2\theta})}, \qquad \text{with} \qquad A_{2\theta} = \frac{\overline{u_k\theta}\,\overline{u_k\theta}}{k\overline{\theta^2}} \tag{12}$$

The equation for dissipation, with the addition of the gravity production term G to the usual shear production P (i.e., using $C_{\varepsilon 3} = 1.$) is written as:

$$\frac{\partial\varepsilon}{\partial t} = \frac{C_{\varepsilon 1}^*(P+G) - C_{\varepsilon 2}\varepsilon}{T} + \frac{\partial}{\partial x_3}\left(\nu + \frac{C_\mu\overline{u_3u_3}T}{\sigma_\varepsilon}\right)\frac{\partial\varepsilon}{\partial x_3} \tag{13}$$

The previous equations and the constants used herein are identical to those of Durbin (1993), except those related to gravity

$$C_1 = 1.22, \quad C_2 = 0.6, \quad C_{\theta 1} = 2.5, \quad C_{\theta 2} = 0.45, \quad C_{\theta 3} = 0.5$$

$$C_{\varepsilon 1}^* = 1.44(1 + a_1 P/\varepsilon), \quad a_1 = 0.1, \quad C_{\varepsilon 2} = 1.9,$$

$$\sigma_k = 1.2, \quad \sigma_\varepsilon = 1.65, \quad \sigma_\theta = 1.5$$

$$C_T = 6.0, \quad C_L = 0.2, \quad C_n = 80$$

Comparison of this model with the lower-Rayleigh case was shown in Boudjemadi et al. (1996). In this case, countergradient transport effects were very large and not captured by either the Daly and Harlow or the Hanjalic and Launder transport models. Good agreement with the DNS was only found by use of an algebraic closure of the triple correlation transport equations in which the effect of the production terms was found large. For the higher-Rayleigh case considered here, the effect of improving these transport models was found not so essential.

Thus, only the results of the simple model described above are displayed in Figure 6. The model yields the following friction and heat transfer results: $u^*/V_b = 1.56\ 10^{-4}$ and $\theta^* = 0.066\,\Delta T$, the latter being 10% larger than the DNS values of $1.63\ 10^{-4}$ and 0.0582. The subsequent results are shown in Figure 6, nondimensionalized with the DNS values of these parameters.

First, the agreement for the *mean velocity* and *temperature* profiles is reasonable. The wall-to-wall heat flux and the shear stress in the core are overestimated by 10%. However, because of the strong and stabilizing coupling between these four variables in this particular flow, they are less sensitive than are the others to changes in the model coefficients. Figure 6a, b include the results of the recent experiments of Betts and Bokhari (1996) at a slightly higher value of $R_a = 8.5\ 10^5$. Agreement with the latter is within the uncertainty of defining u^* and θ^* by extrapolating the experimental results to the wall, assuming a linear profile. A similar agreement is found for the vertical velocity fluctuations (except near the wall, where experiments show slightly more damping). However, the experimental value of the temperature fluctuations is lower than the DNS by nearly 50%.

In Figure 6c, d we note that the wall-normal velocity fluctuation is underpredicted, while the other components are overpredicted. This suggests that the elliptic relaxation is over-representing the blocking of the pressure redistribution by the wall proximity. On the other hand, the wall-normal heat flux is overpredicted, even in the near-wall region. Recall that elliptic relaxation is not applied to the heat fluxes, but present results indicate that it probably should.

Figure 6e shows the budget of the wall-normal Reynolds stress. The homogeneous pressure correlation (Equation 5) is displayed with a dashed line, and the effective pressure correlation resulting from the elliptic operator (Equation 4) is represented by a solid line. The elliptic relaxation performs well in the near-wall layer, but still significantly reduced the return to isotropy effect of the homogeneous model at the center. This effect is much more evident here than in previous channel flow simulations, because the centre of the slot only corresponds to $z^+ = 60$ in standard wall units. This is precisely the range where elliptic relaxation was found effective for channel flows (Wizman et al. 1996).

The *temperature variance* is well reproduced, although its model is simple. On the other hand, the production term of this quantity is nearly exact, because the mean temperature and wall-normal heat flux are quite close to the DNS values. This good agreement of the temperature variance is also a consequence of the good performance of the a priori crude modelling of the corresponding dissipation term (Equations 11, 12). Considering Figure 6f), we notice that kinetic dissipation is not very well represented by the model. Note that the departure from the DNS

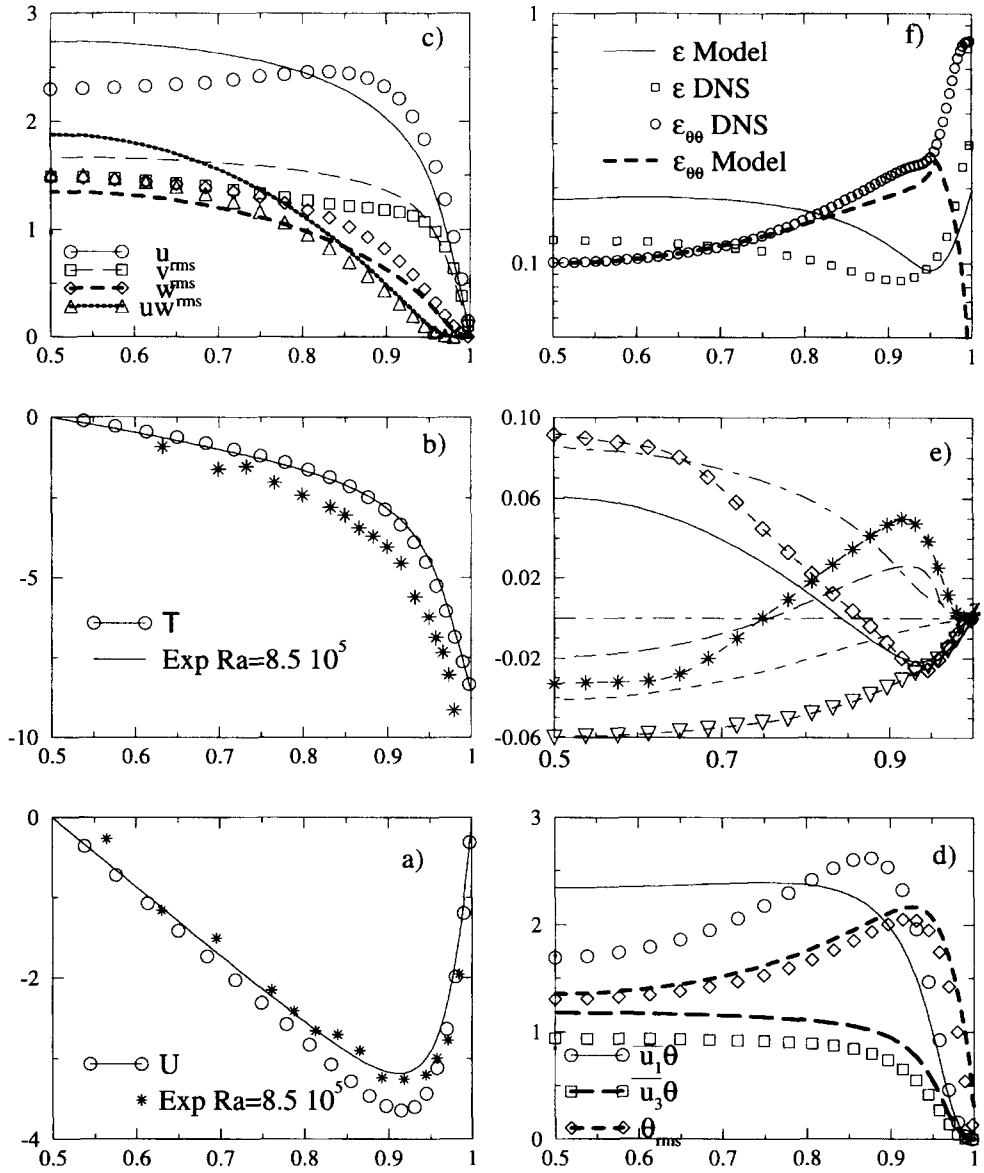

Figure 6 Comparison of model predictions (lines) with DNS (symbols): a) and b) mean velocity and temperature (*; experiments by Betts and Bakhari); c) rms velocity fluctuations and shear stress; d) heat fluxes and rms temperature fluctuations; e) budget of wall-normal Reynolds stress; f) kinetic energy and thermal variance dissipation

curve can be related to the $C^*_{\varepsilon 1}$ function, because (as opposed to what is found in a channel flow for which the model was devised) P/ε does not decrease with increasing distance from the wall. On the other hand, agreement of the thermal dissipation is (perhaps by chance) fairly good (Figure 6). It goes to zero abruptly at the wall as a result of the bound in Equation 9 applied to the time scale T, used also in Equation 11.

Conclusion

The DNS database for the turbulent natural convection flow between infinite differentially heated vertical walls has been analyzed within the scope of second-order modeling. In the absence of gravity stratification (in opposition to *finite* tall enclosures) the flow features are dominated by a quasi-homogeneous shear flow in a wide central region. Gravity, however, still plays a large role through the vertical heat flux generated without a temperature gradient in this direction. Although simple models perform fairly well for these sorts of flows, they actually miss unusual effects, such as negative shear production near the walls, compensated by gravity production.

A straightforward application of a second-moment closure based on elliptic relaxation, although, until now, only tested in nonbuoyant situations, is shown to perform fairly well also. A term-by-term analysis of model and DNS results for the budgets of the second-order correlations budgets shows again that several discrepancies compensate each other.

Because the behavior of these terms in the near-wall layer is different from that of a channel flow, the present case is an interesting candidate for a fine term by term tuning. However, such a task should be undertaken for all terms of the budgets and, because of compensation in the present models, requires further work.

Acknowledgments

The authors acknowledge helpful discussions and comments from the organizers of the 5th ERCOFTAC/IAHR workshop during which the present data were analyzed, and in particular, P. Betts, H. Dol, K. Hanjalic, and B. Launder.

References

Betts, P. and Bokhari H. 1996. New experiments on natural convection in a tall cavity. *Proc. 5th ERCOFTAC-IAHR Workshop on Refined Flow Modelling*. EDF/LNH, Chatou, France

Boudjemadi, R. 1996. Simulation numérique directe et modélisation de la convection naturelle turbulente. Ph.D. thesis, Université de Paris XI, France

Boudjemadi, R., Maupu, V., Laurence, D. and Le Quéré, P. 1996. Direct numerical simulation of free convection in a vertical channel: A tool for second-moment closure modelling. *Proc. 3rd Int. Symposium on Engineering Turbulence Modelling and Measurements*, Crete, Elsevier

Craft, T. J. and Launder, B. E. 1991. Computations of impinging flows using second moment closures, *Proc. 8th Symposium on Turbulent Shear Flows*, Munich, Germany

Durbin, P. A. 1993. A Reynolds-stress model for near-wall turbulence. *J. Fluid Mech.*, **249**, 465–498

Grötzbach, G. and Wörner, M. 1992. Analysis of second-order transport equations by numerical simulations of turbulent convection in liquid metals. *Proc. 5th Int. Topical Meeting on Nuclear Reactor Thermal Hydraulics*, Salt Lake City, UT

Haroutunian, V. and Launder, B. E. 1988. Second-moment modelling of free buoyant shear flows: A comparison of parabolic and elliptic solutions. In *Stably Stratified Flow and Dense Gas Dispersion*, Puttock (ed.), Oxford University Press, New York

Karlsson, R. I., Alavyoon, F. and Eklund, A. 1990. LDV measurements of free convection in electrochemical systems. *Proc. 3rd Int. Conference on Lasr Anemometry*. Springer, Berlin, 329–337

Kasagi, N., Tomita, Y. and Kuroda, A. 1992. Direct numerical simulation of passive scalar field in a turbulent channel flow. *J. Heat Transfer*, **114**, 598–606

Kato, S. Murakami, S. and Yoshie, R. 1993. Experimental and numerical study on natural convection along a heated vertical plate. *Proc. Symposium Turbulent Shear Flow 9*, Kyoto, Japan

Launder, B. E. and Tselepidaleis, D. P. 1991. Progress and paradoxes in modelling near-wall turbulence. *Proc. Symposium Turbulent Shear Flow*, **8**, Munich, Germany

Laurence, D., Dauthieu, I. and Bouchama, N. 1996. *Proc. 5th ERCOFTAC/IAHR Workshop on Refined Flow Modelling*. Chatou-Paris, April 25–26. (Proceedings and database available in electronic format by e-mail request to dominique.laurence@der.edfgdf.fr).

Lee, Y. and Korpela, S. A. 1983. Multicellular natural convection in a vertical slot. *J. Fluid Mech.*, **126**, 91–121

Lyons, S. L., Hanratty, T. J. and McLaughlin, J. B. 1991. Direct numerical simulation of passive heat transfer in a turbulent channel flow. *Int. J. Heat Mass Transfer*, **34**, 1149–1160

Maupu, V., Laurence, D. and Goutorbe, T. 1993. A finite difference direct numerical simulation of passive scalar transport in a turbulent channel flow. *Proc, 5th Int. Symposium on Refined Flow Modelling and Turbulent Measurements*, Paris

Peeters, T. W. J. and Henkes, R. A. W. M. 1992. The Reynolds-stress model of turbulence applied to the natural-convection boundary layer along a heated vertical plate. *Int. J. Heat Mass Transfer*, **35**, 403–420

Phillips, J. R. 1996. Direct simulations of turbulent unstratified natural convection in a vertical slot for Pr = 0.71. *Int. J. Heat Mass Transfer*, **39**, 2485–2494.

Rodi, W. and Mansour, N. 1990. One-equation near-wall turbulence modeling. *Proc. 1990 CTR Summer Program*, Center for Turbulence Research, Stanford University, Stanford, CA

Schumann, V., Schmidt, H. and Volbert, H. 1984. Three-dimensional direct and vectorized elliptic solvers for various boundary conditions. DFVLR-Mitt. 89–15, Germany

So, R. M. C., Lai,, H. S., Zhang, Y. G. and Hwang, B. C. 1991. Second-order, near-wall turbulence closures: A review. *AIAA J.*, **29**

Tsuji, T., Nagano, Y. and Tagawa, M. 1991. Thermally driven turbulent boundary layer. *Proc. 8th Symposium on Turbulent Shear Flow*, Munich

Wizman, V., Laurence, D., Durbin, P., Demuren, A. and Kanniche, M. 1996. Modeling near-wall effects in second-moment closures by elliptic relaxation. to appear in *J. Heat Fluid Flow* (see also *Proc. 10th Turbulent Shear Flow Conf.*, The Pennsylvania University, University Park, PA)